We are IntechOpen,
the world's leading publisher of
Open Access books
Built by scientists, for scientists

6,900
Open access books available

186,000
International authors and editors

200M
Downloads

Our authors are among the

154
Countries delivered to

TOP 1%
most cited scientists

12.2%
Contributors from top 500 universities

Interested in publishing with us?
Contact book.department@intechopen.com

Numbers displayed above are based on latest data collected.
For more information visit www.intechopen.com

Chapter

Synthesis Techniques and Applications of Perovskite Materials

Dinesh Kumar, Ram Sagar Yadav, Monika,

Akhilesh Kumar Singh and Shyam Bahadur Rai

Abstract

Perovskite material is a material with chemical formula ABX_3-type, which exhibits a similar crystal structure of $CaTiO_3$. In this material, A and B are metal cations with ionic valences combined to +6, e.g., Li^+:Nb^{5+}; Ba^{2+}:Ti^{4+}; Sr^{2+}:Mn^{4+}; La^{3+}:Fe^{3+}, and X is an electronegative anion with ionic valence (−2), such as O^{2-}, S^{2-}, etc. The properties of a perovskite material strongly depend on the synthesis route of materials. The perovskite materials may be oxides (ABO_3:$CaMnO_3$), halides (ABX_3: X = Cl, Br, I), nitrides (ABN_3:$CaMoN_3$), sulfides (ABS_3:$LaYS_3$), etc., and they may exist in different forms, such as powders, thin films, etc. There are various routes for the synthesis of several perovskites, such as solid-state synthesis, liquid-state synthesis, gas-state synthesis, etc. In this chapter, we discuss various techniques for the synthesis of oxide perovskites in powder form using solid-, liquid-, and gas-state synthesis methods, and we also present an overview on the other type of perovskite materials. The X-ray diffraction, scanning electron microscopy, and optical techniques are used to study the purity of crystallographic phase, morphology, and photoluminescence properties of the perovskite materials. Some applications of different perovskite materials are also discussed.

Keywords: XRD, perovskite, Rietveld refinement, FullProf Suite, lanthanide phosphor

1. Introduction

The general chemical formula of a perovskite material is ABX_3, which contains a crystal structure similar to $CaTiO_3$. It was initially discovered by German geologist Gustav Rose in 1839 in Ural Mountains, and named after Russian mineralogist Lev Perovski [1, 2]. In ABX_3 perovskite, A and B are termed as metal cations having ionic valences combined to +6, e.g., (Li^+:Nb^{5+}; Ba^{2+}:Ti^{4+}; Sr^{2+}:Mn^{4+}; La^{3+}:Fe^{3+}) and X is an electronegative anion with ionic valence −2 such as O^{2-}, S^{2-} etc. [3–6]. The perovskite materials may be oxides, halides, nitrides, sulfides, etc., and they may exist in different forms, such as powders, thin films, etc. [7–10]. The perovskite material has attracted our attention as it can house up a variety of cations at A- and B-sites individually and/or simultaneously along with anions at X-site [11, 12]. The perovskite materials can be classified in ideal and distorted perovskite materials.

An ideal perovskite material crystallizes into a simple cubic structure with $Pm\overline{3}m$ space group. In the $Pm\overline{3}m$ space group with perovskite structure, A atoms occupy *1(a)* site at (0, 0, 0) and B atoms occupy *1(b)* site at (1/2, 1/2, 1/2) whereas X atoms occupy *3(c)* site at (1/2, 1/2, 0). However, equivalently A, B, and X atoms can also occupy 1(*a*) site at (1/2, 1/2, 1/2), 1(*b*) site at (0, 0, 0) and *3(c)* site at (0, 0, 1/2), respectively, as shown in **Figure 1**. In this figure, A, B, and X are presented in terms of ionic radii [13, 14]. In the unit cell of a perovskite, the cation "B" forms octahedral arrangement with X-anions, i.e., BX_6 and the cation "A" occupies cuboctahedral site with X-anions, i.e., AX_{12}.

The family of perovskite material includes numerous types of oxide forms, such as transition metal oxides with the general formula of ABO_3. The oxide perovskite materials are widely synthesized and are studied for wide applications in various technological fields. In light of these properties, we describe oxide perovskites in more detail.

Victor Moritz Goldschmidt presented an empirical relationship among the ionic radii of A, B, and O, known as tolerance factor (t) to estimate the stability of a perovskite structure. This relation is valid for the relevant ionic radii at room temperature [15]. The numerical value of the tolerance factor can be found by Eq. (1):

$$t = \frac{r_A + r_o}{\sqrt{2}\left(r_B + r_o\right)} \tag{1}$$

where, the term r_A is the ionic radius of cation A and that of r_B is ionic radius of B cation whereas r_O is the ionic radius of oxygen anion (O^{2-}). The ionic radius of A cation is always larger than that of the B cation. The tolerance factor provides an idea about the selection of combination of A and B cations in order to prepare an ideal perovskite material. Eq. (1) can also be expressed in other form, which may be valid for any temperature as given by Eq. (2):

$$t = \frac{d_{A\text{-}o}}{\sqrt{2}\,d_{B\text{-}o}} \tag{2}$$

where d_A-O and d_B-O are average bond-lengths between A-O and B-O, respectively [16].

The distorted perovskite materials are those materials, which crystallize into other than the cubic structures. As far as we know that the perovskite material can accommodate different ions at the A- and B-sites. The variation in the A- and/or B-sites cations causes a variation in the tolerance factor. The variation in tolerance factor leads to a change in the perovskite structure from cubic to non-cubic distorted perovskite structure. For a stable perovskite, the value of tolerance factor should lie in the range of 0.88–1.09 [17]. An ideal perovskite crystal exhibits tolerance factor equal to unity (i.e., t = 1). For t < 1, the perovskite materials show the rhombohedral or monoclinic structure while in the case of t > 1; it reveals tetragonal or orthorhombic structure [18]. Due to distortion in the perovskite system, the BO_6 octahedral led tilted from an ideal situation and causes a change/enhancement in unit cell volume. Thus, the tolerance factor is a measure of the extent of distortion in the perovskite structure. **Figure 2** shows unit cells for some distorted perovskite structures.

There are two general requirements for the formation of a perovskite material, which are given as:

1. **Ionic radii:** the average ionic radii of A- and B-sites cations should be greater than 0.90 Å and 0.51 Å, respectively, and the value of tolerance factor should lie in the range of 0.88–1.09 [19, 20].

2. **Electro-neutrality:** the chemical formula of perovskite material should have neutral balanced charge; consequently, the sum of total charges at A- and B-sites cations must be equal to total charges at O-site (oxygen) of anion(s). A suitable charge distribution is to be achieved in the forms of $A^{3+}B^{3+}O_3$ or $A^{4+}B^{2+}O_3$ or $A^{1+}B^{5+}O_3$ [14, 19].
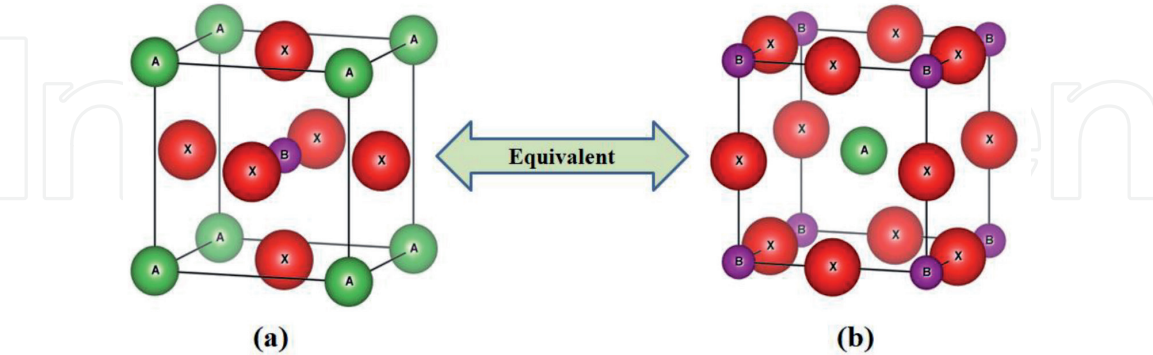
Figure 1.
Molecular structures for ABX_3 perovskite with $Pm\overline{3}m$ space group along with the positions of different atoms in a single unit cell. The figures (a) and (b) are equivalent structures to each other. In the figure (a), A and B take the positions at the corner and body center of the cubic cell, respectively, and X is at the center of face of the unit cell. However, in the figure (b), A and B occupy at body center and the corner of the cubic cell, respectively, and X lies at the center of edge of the unit cell.
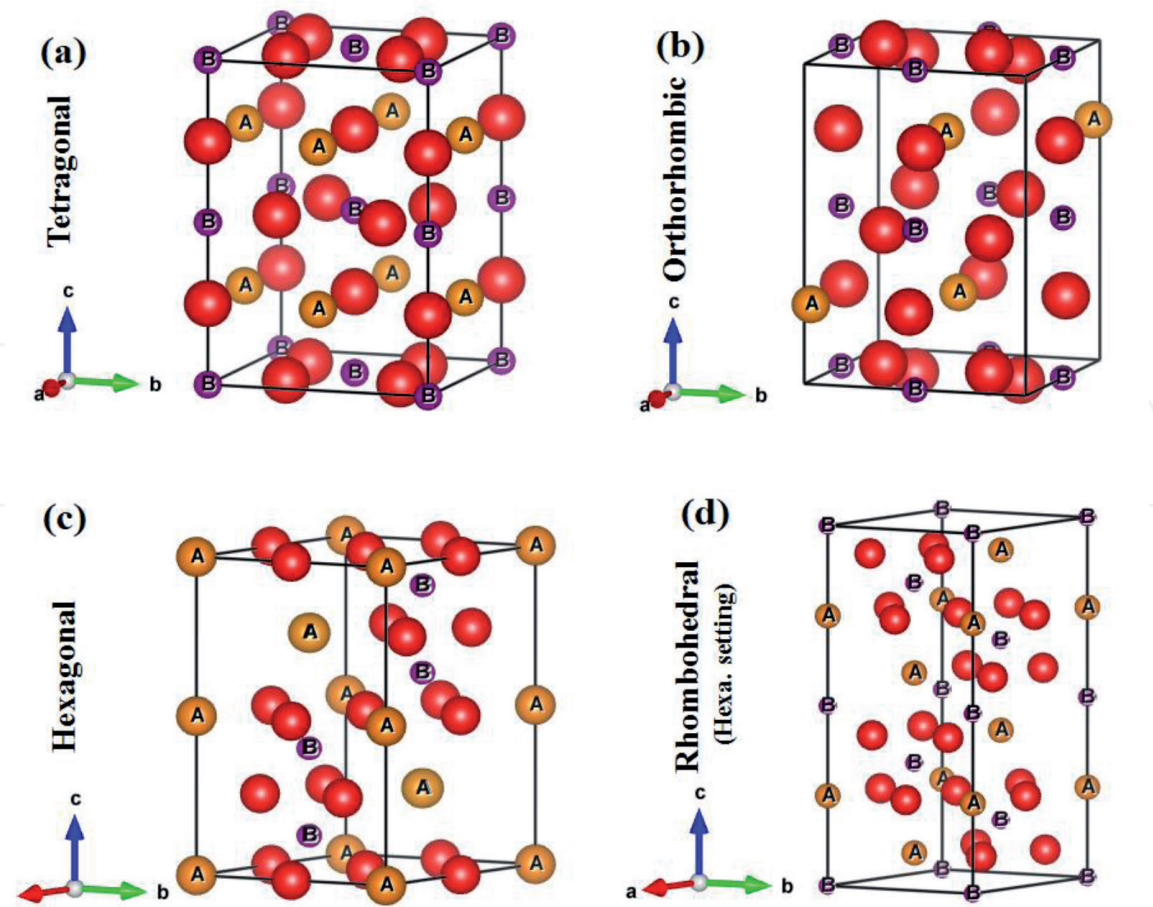
Figure 2.
Different distorted perovskite unit cells; (a) tetragonal, (b) orthorhombic, (c) hexagonal, and (d) rhombohedral. Red spheres stand for oxygen anions.

The pure perovskite materials (ABO_3) do not always provide the desired properties. In order to make them useful, the doping at A- and/or B-sites is required. Doping at A- and/or B-sites improves the properties and also generates very interesting phenomena due to change in crystal structure, bond-lengths, ionic states, etc. The general chemical formula of A- and B-sites after doping in the perovskite matrix may be found in the form of $A_{1-x}A'_xBO_3$ ($0 < x < 1$) and $AB_{1-y}B'_yO_3$ ($0 < y < 1$), respectively. However, the simultaneous A- and B-sites doped oxide perovskites have general formula $A_{1-x}A'_xB_{1-y}B'_yO_3$. Recently, there are several reports on lanthanide-based rare-earth doped perovskites [21–24]. Initially, we discuss the synthesis process used for the preparation of rare-earth doped perovskite materials alongwith their phase identification, structural analysis by Rietveld refinement of X-ray diffraction (XRD) patterns, morphological and optical properties.

2. Synthesis techniques for perovskite materials

As we know that the physical, chemical, and optical properties of the perovskite materials are strongly synthesis route dependent. One has to choose a suitable synthesis method to obtain the desired properties from the prepared materials. Synthesis techniques also affect crystal structure and morphology of the samples [25]. The synthesis techniques can be divided into three main classes as given below:

1. Solid-state synthesis

2. Liquid-state synthesis

3. Gas-state synthesis

These techniques have their own advantages. Solid-state methods are used to synthesize bulk materials, while liquid-state techniques are used to produce nano-materials. However, gas-state methods are mostly used to fabricate thin films. In this, we will discuss these techniques one by one by taking some suitable examples.

2.1 Solid-state synthesis technique

Solid-state synthesis technique is used to produce polycrystalline materials. It is also known as ceramic method because most of the ceramics are synthesized by this method. This is most widely used technique by researchers. This method requires raw materials in carbonates and/or oxides forms. In this method, the raw materials do not react chemically to each-other at room temperature. When the nixture of raw materials is heated at very high temperatures (i.e., 700–1500°C), the chemical reaction takes place at a significant rate.

2.1.1 Mechanical ball-milling method

It is one of the solid-state synthesis methods used for the production of bulk perovskite materials. Synthesis of perovskites using this method involves grinding, hand mixing, ball milling, and firing of starting materials in many times. In this case, the raw materials used in oxides and/or carbonates forms are grinded, hand mixed, ball milled, and calcined at a high temperature.

Let us describe the whole procedure of this synthesis technique by taking an example of $Ca_{0.97-x}TiO_3{:}3Yb^{3+},xBi^{3+}$ perovskite phosphor. For the synthesis of

$CaCO_3$, TiO_2, Yb_2O_3, and Bi_2O_3 were used as the raw materials. First of all, these materials were weighed in the stoichiometric amounts and grinded and mixed by hand in mortor by using pestle for 1–2 h. After hand mixing and grinding of all the starting materials, the mixture was ball milled in a planetary ball milling system to further get homogeneous mixture in the presence of acetone/alcohol as a mixing media for 4–12 h at a nominal rpm (round per minute) of 25–100 in clockwise and anticlockwise directions. After the ball milling, the homogeneous mixture was dried at ordinary temperature and divided into various parts for calcination at different temperatures from 600 to 1500°C for 4–30 h to optimize the pure phase. These phosphors were then structurally and optically characterized [26]. The perovskites prepared using this method have particles size in the submicrometer range [27]. Some other rare earths doped $R_{0.5}Ba_{0.5}CoO_3$ (R = La, Pr, Nd, Sm, Eu, Gd, Tb, Dy) perovskites were also synthesized using this method [28].

2.1.2 High energy ball-milling method

This technique is very similar to that of mechanical ball-milling technique. Only difference is that this method used very high rpm from few hundreds to few thousands for milling with very small sized balls. This technique uses low temperature for the synthesis of the oxide materials. This method produces generally the nanoparticles. This method only takes metal oxides because there is very high possibility of chemical reactions during high energy ball-milling, which may yield different toxic gases.

Now, let us describe the whole process by considering an example of $0.7BiFeO_3$–$0.3PbTiO_3$ (BF-PT) solid solution [29]. The stoichiometric amounts of Bi_2O_3, Fe_2O_3, PbO, and TiO_2 were taken as raw materials to prepare BF-PT and were mixed using agate mortar and pestle. Then the raw materials were ball-milled for 12–30 h with zirconia balls using alcohol as mixing media in the ratio of 1:10 with the sample and balls at 300–1000 rpm. Here, acetone or acid is not used for the purpose of mixing of raw materials as it may damage the milling jars and O-rings. The material dried at 90°C was annealed at various temperatures (i.e., 400–900°C) to optimize the pure phase of the sample. The XRD pattern of the samples was recorded to check the purity of the synthesized perovskite materials.

For additional characterizations, such as dc poling and dielectric measurements, the annealed sample was mixed in 2% aqueous solution of PVA (polyvinyl alcohol) as binder and a pellet was made. The pellet of the perovskites was fired at 500°C for 10–12 h to burn out the PVA binder. Then the pellet was sintered at quite higher temperatures than annealing temperature to obtain the highly dense perovskite material. To further check the purity of the samples after sintering, the XRD pattern was recorded [30]. Sometimes, this method is also used to decrease the particles size from a micrometric scale to nanometric scale. **Figure 3** represents flow chart of the preparation procedures for the synthesis of perovskite materials using solid-state synthesis technique.

2.2 Liquid-state synthesis technique

The liquid-state synthesis technique is a method of synthesis of nanomaterials. It is most widely used by researchers and scientists for the production of nanoparticles of the oxide materials. In this method, the raw materials may be in the form of nitrates, acetates or oxalates, which may react to each other at an ordinary temperature. Auto-combustion, sol-gel, co-precipitation, etc. are different liquid-state synthesis techniques used for the preparation of perovskite nanomaterials, which are to be described in more detail [19].

2.2.1 Auto-combustion method

The auto-combustion synthesis method is a low-cost and very facile technique for the production of perovskite nanomaterials. In this technique, the starting materials are used in oxalates and/or acetates and/or nitrates forms, which are easily soluble in de-ionized water. It involves some organic fuel, such as urea, citric acid, and glycine to assist the combustion.

Let us describe the process of synthesis of the perovskite materials using auto-combustion method (see **Figure 4(a)**) with the help of an example

Figure 3.
A representative flow-chart for the synthesis of oxide materials using ball milling technique.
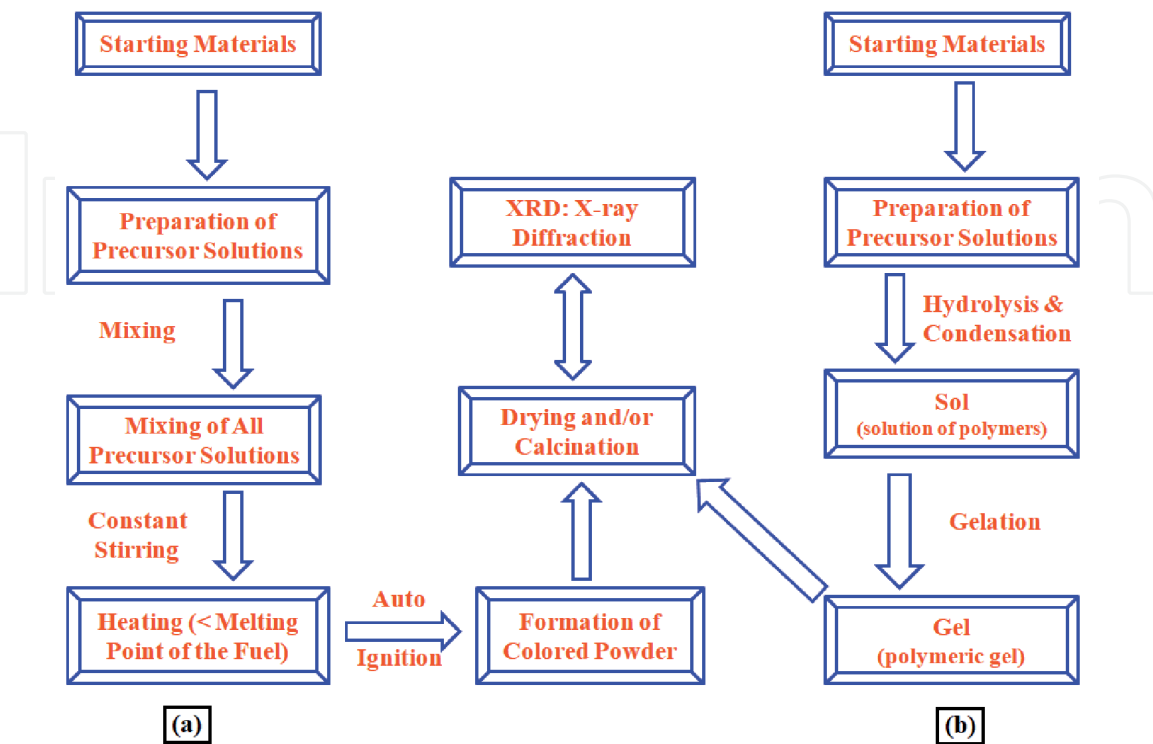

Figure 4.
Schematic flow charts for the synthesis of oxide nanomaterials via (a) auto-combustion and (b) sol-gel methods.

of $La_{0.7}Sr_{0.3}MnO_3$ manganite. Kumar et al. have synthesized $La_{0.7}Sr_{0.3}MnO_3$ perovskite manganite using the starting materials as La_2O_3, $SrCO_3$, and $Mn(CH_3COO)_2.4H_2O$ and glycine was used as fuel. First of all, La_2O_3 and $SrCO_3$ were dissolved in diluted nitric acid to prepare their respective nitrates and then $Mn(CH_3COO)_2.4H_2O$ and glycine were dissolved into distilled water. All the prepared precursor solutions of the materials were dissolved/prepared independently and at the end, they were mixed simultaneously under nonstop stirring in a large beaker and heated on a magnetic stirrer at 175–200°C [31]. After continuous stirring of 6–7 h, the mixed solution became thicker and converted into gel, with further increase in time of stirring, an auto-ignition takes place resulting in flame that evolves huge amount of different gases. During the ignition process, the temperature of the whole mixture may reach upto 800–1000°C for very short time duration. The obtained blackish-brown powder was collected from the beaker and divided into various parts for the calcination at different temperatures. The $La_{0.7}Sr_{0.3}MnO_3$ perovskite comes up with different particles size range. They have also prepared bulk samples of $Ba_{1-x}Sr_xMnO_3$ perovskites using the same method [32]. The $CaTiO_3:Pr^{3+}$, Al^{3+} phosphor was also prepared by Yin et al. using combustion method [33].

2.2.2 Sol-gel method

The sol-gel method is used by most of the chemists for producing nanomaterials. This technique comprises both types of processes (physical and chemical) associated with the following, such as hydrolysis, condensation, polymerization, gelation, drying, and densification [34]. In this technique, the starting materials are used in the form of metal alkoxides. The general chemical formula of metal alkoxides is $M(OR)_x$. Metal alkoxides can be assumed either a derivative of the alcohol ROH, where R is an alkyl group or a derivative of metal hydroxide $M(OH)_x$ [35]. The stoichiometric amounts of metal alkoxides are weighed and dissolved in alcohol or in de-ionized water at a temperature of 60–80°C under steady stirring. It is very important to control the pH value of the metal alkoxides solutions to avoid the formation of the precipitation and to form the homogeneous gel that can be achieved by using basic or acidic solutions. This is known as hydrolysis and condensation leads to form the polymeric chains. The progress of the polymeric chains eventually results to a perceptible improvement in the viscosity of the reaction mixture and the formation of a gel. The obtained gel is to be dried in temperature range between 150 and 200°C to remove the unwanted contents from the gel [35, 36]. After the removal of contents, the obtained gel was annealed at various temperatures in 400–800°C range to obtain the pure phased materials.

Let us discuss the practical processes involve in this technique by taking an example of $La_{0.6}Ca_{0.4}MnO_3$ perovskite. Andrade et al. have synthesized nanotubes and nanoparticles of $La_{0.6}Ca_{0.4}MnO_3$ perovskite manganite using sol-gel method following calcination at different temperatures [37]. They have used stoichiometric amounts of $La(NO_3)_3.6H_2O$, $CaCO_3$ and $Mn(CH_3COO)_2.4H_2O$ for the synthesis of $La_{0.6}Ca_{0.4}MnO_3$ perovskite. The $CaCO_3$ was dissolved in nitric acid to convert into calcium nitrate, while $La(NO_3)_3.6H_2O$ and $Mn(CH_3COO)_2.4H_2O$ were dissolved in distilled water. All the solutions were mixed together in a beaker. The appropriate amount of polyethylene glycol (PEG) was incorporated to the precursor solutions playing the role of polymerizing agent. Then the solution was heated at 70°C for 6 h to complete the polymerization process. At last, the whole solution was converted in yellow viscous gel, which was calcined at different temperatures from 700 to 1000°C. **Figure 4(b)** displays a representative flow chart of the processes involved in the synthesis of perovskite materials using sol-gel method.

2.2.3 Co-precipitation method

The co-precipitation method is also one of the methods used of the production of nanomaterials. This method needs raw materials of metal cations from a general medium and precipitates in the form of oxalates, carbonates, citrates or hydroxides [38–41]. The resultant precipitates are several times washed with distilled water and then obtained product was calcined at various temperatures to acquire the pure phase of the desired materials in the polycrystalline form. This method can yield almost homogeneous polycrystalline powders. The solubility of the used compounds should be very close to each other for a proper precipitation [42]. The precursor solutions are mixed at atomic level resulting lower particles size and it requires very low calcination temperature to get a pure material [43]. The controlling pH of the precursor solution, stirring speed, concentration, and temperature of the mixture are important parameters for the co-precipitation method [44].

The $LaMn_{1-x}Fe_xO_3$ (x = 0, 0.1, 0.2) perovskite synthesized by Geetha et al. is an example of the co-precipitation method [45]. The stoichiometric amounts of $La(NO_3)_3.6H_2O$, $Fe(NO_3)_3.9H_2O$ and $MnCl_2.4H_2O$ were dissolved in distilled water. These solutions were mixed at one platform and stirred continuously at 50°C for 30 min. After this, NaOH solution was added slowly until the pH of solution is attained to 13. The mixed solution of the precursors was again stirred constantly till the formation of black precipitate. The precipitate was collected and washed many times to remove the excess of chlorides and kept in an oven to dry at 50°C. Thus, the final product was calcined at 800°C for 6 h.

It was observed that liquid-state technique produces nanoparticles of perovskite materials at very low temperature. However, the sub-micron sized perovskite materials can be obtained by firing them at higher temperature similar to solid-state technique.

2.3 Gas-state synthesis technique

Gas-state synthesis technique is also used to prepare the nanoparticles. It contains various procedures for the synthesis of powder oxide materials, viz. furnaces, flames, plasmas, and lasers. The basics of thermodynamics and kinetics of the reaction are very similar to each other; however, their reactors are different. These methods provide narrow distribution of the nanoparticles. The dispersion must be reduced for narrow distribution of the nanoparticles as it leads to increase the particles size [25]. Gas-state synthesis technique is a bottom-up method for the synthesis of multifunctional nanoparticles. Method of bottom-up nanofabrication is based on the gathering of nanomaterials from smaller components.

A variety of electronic devices and solar cells of perovskite materials are prepared in terms of thin films via these techniques and they are entirely different from the other synthesis techniques. There are various techniques for the preparation of thin films, such as chemical vapor deposition [46], molecular beam epitaxy [47], laser ablation [48], DC sputtering [49], magnetron sputtering [50], thermal evaporation [51], and electron beam evaporation [52]. The gas-state synthesis method needs particular set up for a good quality of samples to offer the preferred properties. The gas-state synthesis techniques are categorized into three types:

a. Fabrication at the crystallization temperature under a suitable atmosphere condition of temperature.

b. Fabrication in an intermediate temperature range (500–800°C) followed by post-annealing treatment at higher temperatures.

c. Fabrication at a very low substrate temperature followed by post-annealing treatment at very high temperature.

The perovskite materials fabricated using gas-state techniques have variety of applications ranging from optical and anticorrosion coatings to photocatalysts and solar cells, from semiconductor devices to capacitor dielectrics, from bio-implantable devices to chemical reactors and catalysts. One can undoubtedly say that the industrial interest for preparing nanomaterial-based technologies through gas-state synthesis is going to increase in the upcoming years.

3. Structural and optical properties

3.1 Identification of phase purity: X-ray diffraction studies

It is very important to check the phase and its purity of synthesized perovskite materials. Without knowing the phase purity, one cannot come to any conclusion about the properties exhibited by the perovskite materials. The XRD technique is a suitable tool to identify the phase of perovskites. From the XRD data, one can find out relative phase fractions of different phases present in the prepared samples. One can also find out lattice constants, unit cell volume, crystallite size, lattice strain, and theoretical density from Rietveld refinement of the XRD pattern. The XRD technique is also used to optimize the synthesis conditions for the perovskite materials. By matching the XRD pattern of the synthesized material with the standard XRD pattern of the cubic phase of $CaTiO_3$ (CT) perovskite, one can conclude about the phase purity, i.e., whether, the perovskite is pure or has some amount of impurity phase(s) or crystallizes in the distorted perovskite. **Figure 5** shows the XRD pattern of the cubic CT perovskite with JCPDS File No. 75-2100 using X-ray radiation of 1.5406 Å wavelength. The analysis of XRD pattern gives unit cell lattice parameter a = 3.795 Å and unit cell volume V = 54.656 Å^3. An ideal perovskite material displays reflections from all allowed planes of the primitive unit cell. It shows most intense XRD peak for (1 1 0) plane in the 2θ range of 32–34° and first singlet reflection corresponding to (1 0 0) plane between 22 and 24°.
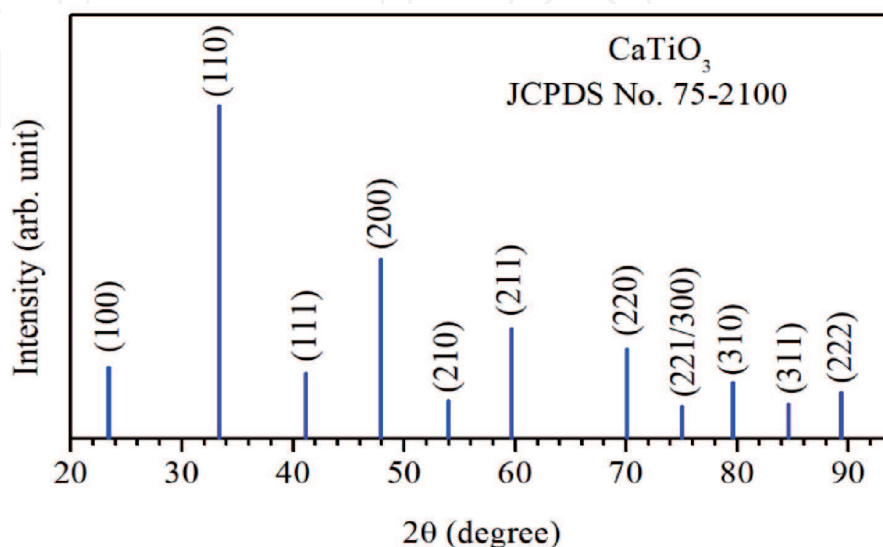

Figure 5.
The standard XRD pattern for the cubic phase of $CaTiO_3$ perovskite.

As we know that the different materials display different XRD patterns as like the finger print of the humans. However, a certain prototype of materials gives the XRD pattern in a well-defined manner. In order to make sure that the synthesized sample is perovskite or not, we have to match the XRD pattern of the synthesized sample with the XRD pattern of CT. If it matches it forms a perovskite phase otherwise not.

Figure 6(a) shows the room-temperature XRD pattern for $BaTiO_3$ (BT) synthesized by mechanical ball-milling method followed by calcination at 950°C for 5 h and it is compared with XRD pattern of CT. The comparison of both the XRD patterns reveals that the XRD pattern of BT matches with that of the CT. This further confirms that BT is a perovskite material. The Bragg's peaks in XRD pattern of BT perovskite is shifted towards lower angle side compared to CT. This indicates that the lattice parameters of BT are larger than that of the CT. Furthermore, the Bragg peak around 22° is asymmetric in lower angle side, which shows doublet nature in the peak, i.e., the lattice plane (1 0 0) of CT split into (0 0 1) and (1 0 0) of BT is shown as inset in **Figure 6(a)**. Similarly, the other Bragg's peaks also show asymmetrical behavior. All these observations reveal that the crystal structure of BT is distorted from an ideal perovskite structure. The Rietveld refinement of XRD pattern of BT reveals that the BT crystallizes into tetragonally distorted structure with *P4mm* space group [53]. It has been also observed that the presence of superlattice reflection(s) in the XRD pattern indicates the formation of distorted perovskite structure from an ideal cubic [54, 55]. The structural analysis of the known or unknown perovskite materials can be identified by Rietveld refinement of the powder XRD pattern with the help of some standard software [56]. Most of researchers use FullProf Suite to identify the structure of various perovskite materials [57]. From Rietveld refinement, one can get lattice parameters, atomic coordinates of the constituent atoms present in the unit cell, average bond-lengths and angles, draw molecular structure to see the surroundings of the A- and B-sites' cations with anions, and many more [29, 33, 58]. One can also find out magnetic structure from the Rietveld refinement of the neutron diffraction data [59].

We performed the Rietveld refinement of XRD pattern of BT using *P4mm* space group of the tetragonal structure. In *P4mm* space group, Ti^{4+}-ions and Ba^{2+}-ions occupy *1(a)* site at (0, 0, 0) and *1(b)* site at (0.5, 0.5, 0.5 + δz), respectively, while, O^{2-}(1) and O^{2-}(2) anions substitute *1(a)* site at (0, 0, 0.5 + δz) and *2(c)* site at (0.5, 0, δz), respectively [53, 60]. The structural analysis provides
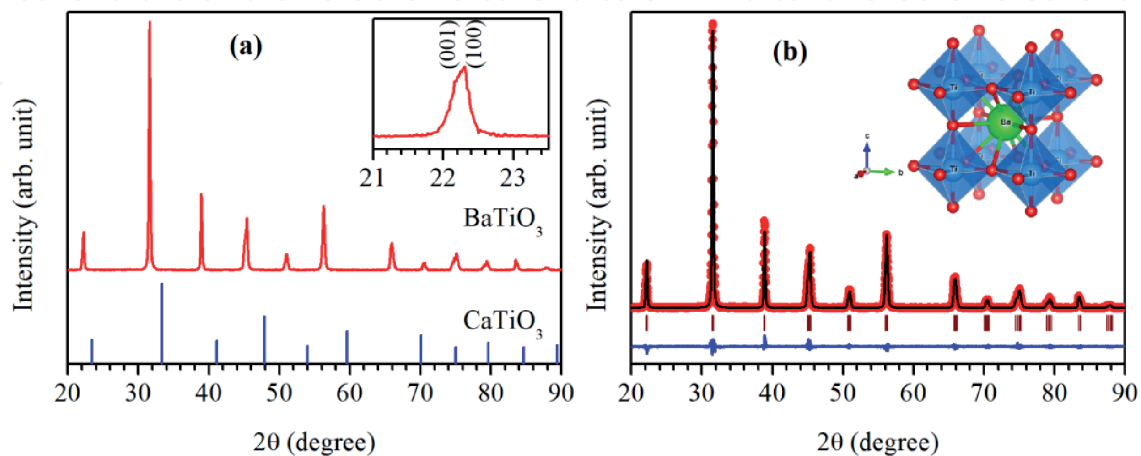

Figure 6.
(a) Room temperature XRD pattern of $BaTiO_3$ compared with the $CaTiO_3$. The inset in (a) shows selected Bragg's peak between 21.0 and 23.5°. (b) Rietveld fit of the XRD pattern of $BaTiO_3$. The inset in (b) shows ball and stick molecular model for the unit cell of $BaTiO_3$ perovskite, where Ba, Ti, and O are present in their atomic sizes.

lattice constants a = b = 4.0005(1) Å and c = 4.0255(2) Å and unit cell volume V = 64.423(4) Å^3 with tetragonality (c/a) of 1.006 close to the earlier reported value [60]. **Figure 6(b)** shows Rietveld fit of the XRD pattern for the BT perovskite. In this figure, the scattered dots are used to present experimental XRD pattern and continuous line over experimental pattern is to show the simulated XRD pattern. Lower continuous curve shows difference between experimental and simulated XRD patterns. The vertical bars represent positions of the Bragg's reflection. The inset of **Figure 6(b)** demonstrates ball and stick molecular model for the unit cell of *P4mm* space group for BT in terms of atomic sizes. It is clear that Ba atom forms octahedral with oxygen atoms (BaO$_6$) and Ti atom forms cubocta-hedral with oxygen atoms (TiO$_{12}$).

3.2 Morphological studies

The scanning electron microscopy (SEM) and transmission electron microscopy (TEM) can be used to study the microstructure nature of the perovskite materials. We have recorded SEM micrographs of Nd$_{0.4}$Sr$_{0.6}$MnO$_3$ manganite samples calcined at 800°C and 1200°C synthesized by auto-combustion method using FEI, Nova Nano SEM for the Nd$_{0.4}$Sr$_{0.6}$MnO$_3$ perovskite and they are shown in **Figure 7**. The average values of the particle size were analyzed by ImageJ software and they are found to be 50 and 425 nm for the Nd$_{0.4}$Sr$_{0.6}$MnO$_3$ perovskites calcined at 800°C and 1200°C, respectively. This clearly shows that the average particle size improves on increasing the calcination temperature. It confirms that the sample calcined at 800°C produces nanomaterial whereas that of at 1200°C gives bulk material.

3.3 Optical studies

Figure 8 shows photoluminescence (PL) excitation and PL emission spectra of the Nd$_{0.4}$Sr$_{0.6}$MnO$_3$ manganite calcined at 800°C and 1200°C. **Figure 8(a)** shows the excitation spectra of the Nd$_{0.4}$Sr$_{0.6}$MnO$_3$ manganite in both the cases and contains an intense peak at 355 nm [45]. It was monitored at an emission wavelength of 646 nm. The intensity of bulk material is two times larger than the nanomaterial. When both the materials were excited with 355 nm they give strong red color at 646 nm as shown in **Figure 8(b)**. It also contains weak peaks at 483 and 582 nm. The emission intensity obtained in the case of bulk material is further two times larger than the nanomaterial. This is due to the increase in crystallinity and particles size of the materials. Thus, the calcination affects the morphology and optical properties of perovskites even though the perovskite material was synthesized by auto-combustion method.
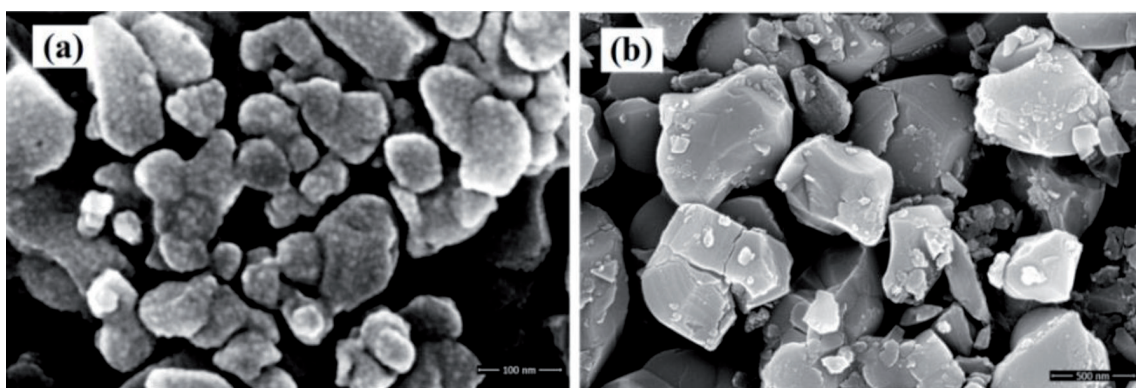

Figure 7.
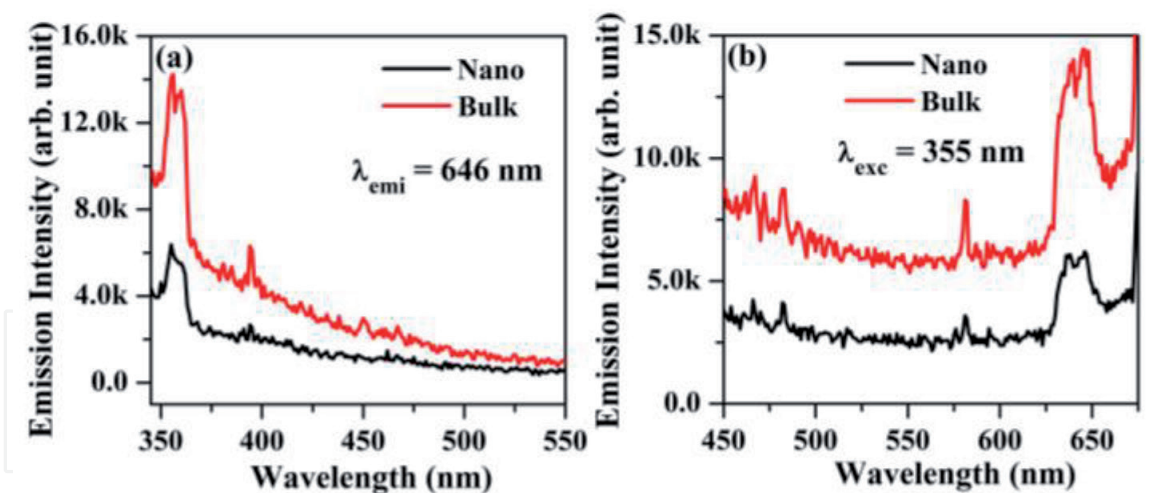*SEM micrographs of Nd$_{0.4}$Sr$_{0.6}$MnO$_3$ manganite calcined at (a) 800°C and (b) 1200°C temperatures.*

Figure 8.
(a) PL excitation and (b) PL emission spectra of the $Nd_{0.4}Sr_{0.6}MnO_3$ manganite calcined at 800°C and 1200°C temperatures.

4. Applications of perovskite materials

The perovskite materials are extensively studied by researchers due to their attractive properties. The perovskite materials have wide applications in various fields, which are listed below:

1. Photocatalytic activity; e.g., $LaFeO_3$ [61].

2. Photovoltaic solar cells; e.g., $LaVO_3$ [62].

3. Phosphor materials in photoluminescence; e.g., $Ho^{3+}/Yb^{3+}/Mg^{2+}$ doped $CaZrO_3$ [63].

4. Solid oxide fuel cells; e.g., $Gd_{0.7}Ca_{0.3}Co_{1-y}Mn_yO_3$ [64].

5. Sensors and actuators; e.g., $PbZr_xTi_1$-xO_3 [65].

6. Magnetic memory devices; e.g., $Pt/La_2Co_{0.8}Mn_{1.2}O_6/Nb:SrTiO_3$ [66].

7. Magnetic field sensors; e.g., $La_{0.67}Sr_{0.33}MnO_3$ and $La_{0.67}Ba_{0.33}MnO_3$ [67].

8. Electric field effect devices; e.g., hetrostructure of $Pb(Zr_{0.2}Ti_{0.8})O_3/La_{0.8}Ca_{0.2}MnO_3$ [68].

9. Ferroelectric and piezoelectric devices; e.g., $BaTiO_3$, $PbTiO_3$ [69].

10. Semiconducting electronic devices; e.g., $La_{0.7}Ca_{0.3}MnO_3/SrTiO_3/La_{0.7}Ce_{0.3}MnO_3$ [70].

11. High dielectric constant; e.g., Bi_1-xSr_xMnO_3 (x = 0.4, 0.5) [71].

12. High temperature superconductor; e.g., $BaPb_1$-xBi_xO_3 [72].

13. Hypothermia; e.g., $La_{0.7}Sr_{0.3}MnO_3$ [73].

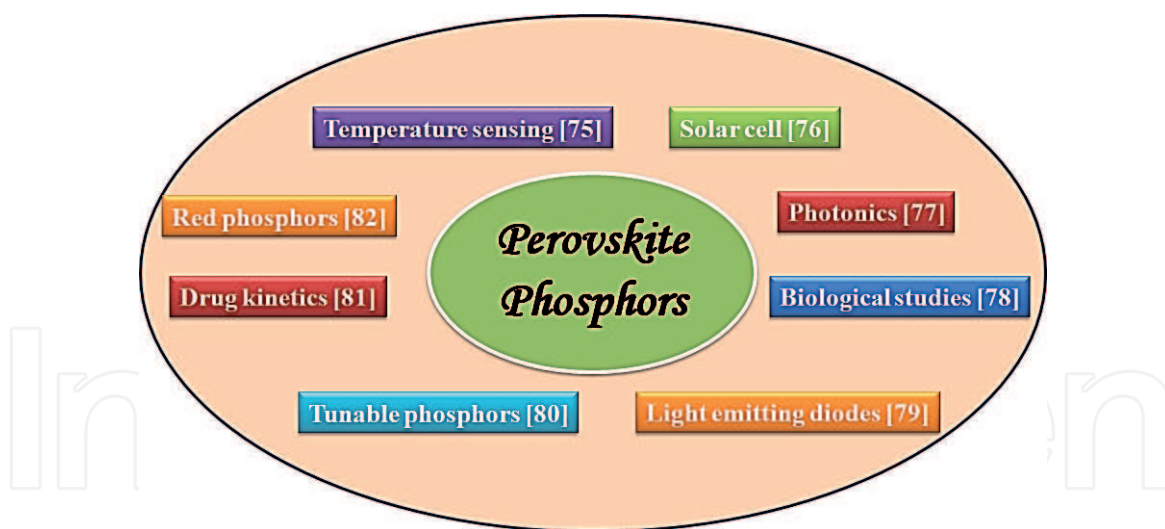14. Supercapacitor; e.g., $KNi_{0.8}Co_{0.2}F_3$ [74].

Figure 9.
Block diagram of the lanthanide based perovskite phosphor materials including their applications in various fields [75–82].

The lanthanide based perovskite phosphors are one of them and have unique photolumincence properties. The lanthanide ions are known for their narrow and sharp band emissions. They give emissions in the entire range of visible spectrum along with ultraviolet (UV) and near infrared (NIR) regions. These emissions are observed due to presence of meta-stable energy levels in the lanthanide ions. These levels have long lifetime and are responsible for very strong emissions. The lanthanide ions possess upconversion, downconversion, and quantum cutting phenomena. In upconversion, the two or more than two low energy photons are converted into high energy photons. When a high energy photon is converted into low energy photons it is termed as downconversion process. However, in quantun cutting, a high energy photon is converted into two low energy NIR photons. These processes lead numerous technological applications in different fields, such as red phosphors, light emitting diodes (LEDs), photonics, solar cells, tunable phosphors, temperature sensing, biological studies, drug kinetics, etc. [63, 75–82]. **Figure 9** shows a block diagram for the lanthanide based perovskite phosphors, which shows their applications in various fields.

5. Conclusions

This chapter summarizes the basics of the perovskite structure, its stability and distortion. We have discussed the novelty of the perovskite materials, which accommodate different cations at A- and/or B-sites individually and/or simultaneously. We have also discussed various routes such as solid, liquid and gas-state synthesis for the preparation of perovskite materials mostly in the oxide powder forms. We have also briefly described the phase identification of the perovskites and their structural analysis using Rietveld refinement of the XRD data by taking an example of tetragonal $BaTiO_3$ perovskite. The morphological and optical studies were also incorporated. We have also briefly listed various applications of perovskite materials including lanthanide based perovskite phosphors in various fields.

Conflict of interest

The authors declare no conflict of interest in the chapter.

Author details

Dinesh Kumar[1], Ram Sagar Yadav[2*], Monika[3], Akhilesh Kumar Singh[1] and Shyam Bahadur Rai[3]

1 School of Materials Science and Technology, Indian Institute of Technology, Banaras Hindu University, Varanasi, Uttar Pradesh, India

2 Department of Zoology, Institute of Science, Banaras Hindu University, Varanasi, Uttar Pradesh, India

3 Department of Physics, Institute of Science, Banaras Hindu University, Varanasi, Uttar Pradesh, India

*Address all correspondence to: ramsagaryadav@gmail.com

IntechOpen

References

[1] Roth RS. Classification of perovskite and other ABO_3-type compounds. Journal of Research of the National Bureau of Standards. 1957;**58**:75-88

[2] Yashima M, Ali R. Structural phase transition and octahedral tilting in the calcium titanate perovskite $CaTiO_3$. Solid State Ionics. 2009;**180**:120-126

[3] Weis RS, Gaylord TK. Lithium niobate: Summary of physical properties and crystal structure. Applied Physics A: Materials Science & Processing. 1985;**37**:191-203

[4] Kwei GH, Lawson AC, Billinge SJL, Cheong SW. Structures of the ferroelectric phases of barium titanate. The Journal of Physical Chemistry. 1993;**97**:2368-2377

[5] Sakai H, Ishiwata S, Okuyama D, Nakao A, Nakao H, Murakami Y, et al. Electron doping in the cubic perovskite $SrMnO_3$: Isotropic metal versus chainlike ordering of Jahn-Teller polarons. Physical Review B. 2010;**82**:180409R–180412R

[6] Wang Y, Zhu J, Zhang L, Yang X, Lu L, Wang X. Preparation and characterization of perovskite $LaFeO_3$ nanocrystals. Materials Letters. 2006;**60**:1767-1770

[7] Kubicek M, Bork AH, Rupp JLM. Perovskite oxides—A review on a versatile material class for solar-to-fuel conversion processes. Journal of Materials Chemistry A. 2017;**5**:11983-12000

[8] Protesescu L, Yakunin S, Bodnarchuk MI, Krieg F, Caputo R, Hendon CH, et al. Nanocrystals of cesium lead halide perovskites ($CsPbX_3$, X = Cl, Br, and I): Novel optoelectronic materials showing bright emission with wide color gamut. Nano Letters. 2015;**15**:3692-3696

[9] Perez RS, Cerqueira TFT, Korbel S, Botti S, Marques MAL. Prediction of stable nitride perovskites. Chemistry of Materials. 2015;**27**:5957-5963

[10] Kuhar K, Crovetto A, Pandey M, Thygesen KS, Seger B, Vesborg PCK, et al. Sulfide perovskites for solar energy conversion applications: Computational screening and synthesis of the selected compound $LaYS_3$. Energy & Environmental Science. 2017;**10**:2579-2593

[11] Kansara SB, Dhruv D, Kataria B, Thaker CM, Rayaprol S, Prajapat CL, et al. Structural, transport and magnetic properties of monovalent doped $La_{1-x}Na_xMnO_3$ manganites. Ceramics International. 2015;**41**:7162-7173

[12] Pandey R, Pillutla RK, Shankar U, Singh AK. Absence of tetragonal distortion in $(1-x)SrTiO_{3-x}Bi(Zn_{1/2}Ti_{1/2})O_3$ solid solution. Journal of Applied Physics. 2013;**113**:184109-184114

[13] Ali Z, Ahmad I, Amin B, Maqbool M, Murtaza G, Khan I, et al. Theoretical studies of structural and magnetic properties of cubic perovskites $PrCoO_3$ and $NdCoO_3$. Physica B. 2011;**406**:3800-3804

[14] Johnsson M, Lemmens P. Crystallography and chemistry of perovskites. In: Kronmuller H, Parkin S, editors. Handbook of Magnetism and Advanced Magnetic Materials. Vol. 4. USA: John Wiley & Sons; 2005. pp. 1-11

[15] Goldschmidt VM. Die Gesetze der Krystallochemie. Naturwissenschaften. 1926;**14**:477-485

[16] Kumar D, Verma NK, Singh CB, Singh AK. Evolution of structural characteristics of $Nd_{0.7}Ba_{0.3}MnO_3$ perovskite manganite as a function of crystallite size. AIP Conference Proceedings. 2018 2009:020013-4

[17] Duan R. High curie temperature bismuth- and indium-substituted lead titanate [thesis]. Georgia Institute of Technology: School of Materials Science and Engineering; 2004

[18] Kumar D, Singh AK. Investigation of structural and magnetic properties of $Nd_{0.7}Ba_{0.3}Mn_{1-x}Ti_xO_3$ (x = 0.05, 0.15 and 0.25) manganites synthesized through a single-step process. Journal of Magnetism and Magnetic Materials. 2019;**469**:264-273

[19] Atta NF, Galal A, El-Ads EH. Synthesis, characterization and applications. In: Pan L, Zhu G, editors. Perovskite Nanomaterials. London: IntechOpen; 2016. pp. 107-151. Ch. 4

[20] Porta P, De RS, Faticanti M, Minelli G, Pettiti I, Lisi L, et al. Perovskite-type oxides: I. Structural, magnetic, and morphological properties of $LaMn_{1-x}Cu_xO_3$ and $LaCo_{1-x}Cu_xO_3$ solid solutions with large surface area. Journal of Solid State Chemistry. 1999;**146**:291-304

[21] Chen M, Zhang H, Liu T, Jiang H, Chang A. Preparation, structure and electrical properties of $La_{1-x}Ba_xCrO_3NTC$ ceramics. Journal of Materials Science: Materials in Electronics. 2017;**28**:18873-18188

[22] Yang J, Ma YQ, Zhang RL, Zhao BC, Ang R, Song WH, et al. Structural, transport, and magnetic properties in the Ti-doped manganites $LaMn_{1-x}Ti_xO_3$ ($0 \leq x \leq 0.2$). Solid State Communications. 2005;**136**:268-272

[23] Kameli P, Salamati H, Heidarian A, Bahrami H. Ferromagnetic insulating and reentrant spin glass behavior in Mg doped $La_{0.75}Sr_{0.25}MnO_3$ manganites. Journal of Non-Crystalline Solids. 2009;**355**:917-921

[24] Choudhary N, Verma MK, Sharma ND, Sharma S, Singh D. Correlation between magnetic and transport properties of rare earth doped perovskite manganites $La_{0.6}R_{0.1}Ca_{0.3}MnO_3$ (R = La, Nd, Sm, Gd, and Dy) synthesized by Pechini process. Materials Chemistry and Physics. 2020;**242**:122482 pp. 11

[25] Ring TA. Fundamentals of Ceramic Powder Processing and Synthesis: Ceramic Powder Synthesis. United States: Academic Press; 1996

[26] Lin L-T, Chen J-Q, Deng C, Tang L, Chen D-J, Meng J-X, et al. Broadband near-infrared quantum-cutting by cooperative energy transfer in Yb^{3+}–Bi^{3+} co-doped $CaTiO_3$ for solar cells. Journal of Alloys and Compounds. 2015;**640**:280-284

[27] Pandey R, Tiwari A, Upadhyay A, Singh AK. Phase coexistence and the structure of the morphotropic phase boundary region in $(1-x)Bi(Mg_{1/2}Zr_{1/2})O_3$-$xPbTiO_3$ piezoceramics. Acta Materialia. 2014;**76**:198-206

[28] Troyanchuk IO, Kasper NV, Khalyavin DD, Szymczak H, Szymczak R, Baran M. Magnetic and electrical transport properties of orthocobaltites $R_{0.5}Ba_{0.5}CoO_3$ (R = La, Pr, Nd, Sm, Eu, Gd, Tb, Dy). Physical Review B. 1998;**58**:2418-2421

[29] Zhang L, Xu Z, Cao L, Yao X. Synthesis of BF-PT perovskite powders by high-energy ball milling. Materials Letters. 2007;**61**:1130-1133

[30] Upadhyay A, Pandey R, Singh AK. Origin of ferroelectric P-E loop in cubic compositions and structure of poled $(1-x)Bi(Mg_{1/2}Zr_{1/2})O_3$-$xPbTiO_3$ piezoceramics. Journal of the American Ceramic Society. 2017;**100**:1743-1750

[31] Kumar D, Verma NK, Singh CB, Singh AK. Crystallite size strain analysis of nanocrystalline $La_{0.7}Sr_{0.3}MnO_3$ perovskite by Williamson-Hall plot method. AIP Conference Proceedings. 2018 1942:050024-4

[32] Kumar D, Singh CB, Verma NK, Singh AK. Synthesis and structural investigations on multiferroic $Ba_{1-x}Sr_xMnO_3$ perovskite manganites. Ferroelectrics. 2017;**518**:191-195

[33] Yin S, Chen D, Tang W. Combustion synthesis and luminescent properties of $CaTiO_3$:Pr, Al persistent phosphors. Journal of Alloys and Compounds. 2007;**441**:327-331

[34] Brinker CJ, Scherer GW. Sol-Gel Science: The Physics and the Chemistry of Sol-Gel Processing. London: Academic Press Inc.; 1990

[35] Rahaman MN. Ceramic Processing and Sintering. 2nd ed. New York: Marcel Dekker Inc.; 2003

[36] Rajaeiyan A, Mohagheghi MMB. Comparison of sol-gel and co-precipitation methods on the structural properties and phase transformation of γ and α-Al_2O_3 nanoparticles. Advanced Manufacturing. 2013;**1**:176-182

[37] Andrade VM, Vivas RJC, Pedro SS, Tedesco JCG, Rossi AL, Coelho AA, et al. Magnetic and magnetocaloric properties of $La_{0.6}Ca_{0.4}MnO_3$ tunable by particle size and dimensionality. Acta Materialia. 2016;**102**:49-55

[38] Pei RR, Chen X, Suo Y, Xiao T, Ge QQ, Yao HC, et al. Synthesis of $La_{0.85}Sr_{0.15}Ga_{0.8}Mg_{0.2}O_3$-$\delta$ powder by carbonate co-precipitation combining with azeotropic-distillation process. Solid State Ionics. 2012;**219**:34-40

[39] Uskokovic V, Drofenik M. Four novel co-precipitation procedures for the synthesis of lanthanum-strontium manganites. Materials and Design. 2007;**28**:667-672

[40] Cho TH, Shiosaki Y, Noguchi H. Preparation and characterization of layered $LiMn_{1/3}Ni_{1/3}Co_{1/3}O_2$ as a cathode material by an oxalate co-precipitation method. Journal of Power Sources. 2006;**159**:1322-1327

[41] Wei Y, Han B, Hu X, Lin Y, Wang X, Deng X. Synthesis of Fe_3O_4 nanoparticles and their magnetic properties. Procedia Engineering. 2012;**27**:632-637

[42] West AR. Solid State Chemistry and its Applications. USA: John Wiley & Sons; 2005

[43] Gaikwad AB, Navale SC, Samuel V, Murugan AV, Ravi V. A co-precipitation technique to prepare $BiNbO_4$, $MgTiO_3$ and $Mg_4Ta_2O_9$ powders. Materials Research Bulletin. 2006;**41**:347-353

[44] Zawrah MF, Hamaad H, Meky S. Synthesis and characterization of nano $MgAl_2O_4$ spinel by the co-precipitated method. Ceramics International. 2007;**33**:969-978

[45] Geetha N, Senthil KV, Prakash D. Synthesis and characterization of $LaMn_{1-x}Fe_xO_3$ (x = 0, 0.1, 0.2) by coprecipitation route. Journal of Physical Chemistry & Biophysics. 2018;**8**:273-278

[46] Kwak BS, Zhang K, Boyd EP, Erbil A, Wilkens BJ. Metalorganic chemical vapor deposition of $BaTiO_3$ thin films. Journal of Applied Physics. 1991;**69**:767-772

[47] Yu Z, Ramdani J, Curless JA, Finder JM, Overgaard CD, Droopad R, et al. Epitaxial perovskite thin films grown on silicon by molecular beam epitaxy. Journal of Vacuum Science and Technology B. 2000;**18**:1653-1657

[48] Imai T, Okuyama M, Hamakawa Y. $PbTiO_3$ thin films deposited by laser ablation. Japanese Journal of Applied Physics. 1991;**30**:2163-2166

[49] Bangchao Y, Wang JY, Jia YM, Yongjie H. Preparation of $PbTiO_3$ thin film by dc single-target magnetron

sputtering. Proceedings of the SPIE. 1991;**1519**:725-728

[50] Lu CJ, Shen HM, Wang YN. Preparation and crystallization of $Pb(Zr_{0.95}Ti_{0.05})O_3$ thin films deposited by radio-frequency magnetron sputtering with a stoichiometric ceramic target. Applied Physics A: Materials Science and Processing. 1998;**67**:253-258

[51] Li Y, Xu X, Wang C, Wang C, Xie F, Yang J, et al. Investigation on thermal evaporated $CH_3NH_3PbI_3$ thin films. AIP Advances. 2015;**5**:097111-097116

[52] Pae SR, Byun S, Kim J, Kim M, Gereige I, Shin B. Improving uniformity and reproducibility of hybrid perovskite solar cells via a low-temperature vacuum deposition process for NiO_x hole transport layers. ACS Applied Materials & Interfaces. 2018;**10**:534-540

[53] Xiao CJ, Jin CQ, Wang XH. Crystal structure of dense nanocrystalline $BaTiO_3$ ceramics. Materials Chemistry and Physics. 2008;**111**:209-212

[54] Geller S. Crystal structure of gadolinium orthoferrite $GdFeO_3$. The Journal of Chemical Physics. 1956;**24**:1236-1239

[55] Jakymiw C, Vocadlo L, Dobson DP, Bailey E, Thomson AR, Brodholt JP, et al. The phase diagrams of $KCaF_3$ and $NaMgF_3$ by *ab initio* simulations. Physics and Chemistry of Minerals. 2018;**45**:311-322

[56] Young RA. The Rietveld Method. International Union of Crystallography: Oxford University Press; 1993

[57] Carvajal JR. 'FULLPROF' Program: Rietveld Pattern Matching Analysis of Powder Patterns-ILL. Grenoble; 1990

[58] Yadav RS, Kumar D, Singh AK, Rai E, Rai SB. Effect of Bi^{3+} ion on upconversion-based induced optical heating and temperature sensing characteristics in the Er^{3+}/Yb^{3+} co-doped La_2O_3 nano-phosphor. RSC Advances. 2018;**8**:34699-34711

[59] Carvajal JR. Recent advances in magnetic structure determination by neutron powder diffraction. Physica B. 1993;**192**:55-69

[60] Villars P. Pauling file in: Inorganic Solid Phases. Springer Materials (online database). Springer Materials. $BaTiO_3$ tetragonal ($BaTiO_3$ rt) Crystal Structure. Heidelberg: Springer. Available from: https://materials. springer.com/isp/crystallographic/docs/ sd_1626689

[61] Afifah N, Saleh R. Enhancement of photocatalytic activities of perovskite $LaFeO_3$ composite by incorporating nanographene platelets. IOP Conference Series: Materials Science and Engineering. 2017;**188**:012054-012058

[62] Wang L, Li Y, Bera A, Ma C, Jin F, Yuan K, et al. Device performance of the Mott insulator $LaVO_3$ as a photovoltaic material. Physical Review Applied. 2015;**3**:064015-064029

[63] Maurya A, Yadav RS, Yadav RV, Rai SB, Bahadur A. Enhanced green upconversion photoluminescence from Ho^{3+}/Yb^{3+} co-doped $CaZrO_3$ phosphor via Mg^{2+} doping. RSC Advances. 2016;**6**:113469-113477

[64] Skinner SJ. Recent advances in perovskite-type materials for solid oxide fuel cell cathodes. International Journal of Inorganic Materials. 2001;**3**:113-121

[65] Uchino K. Glory of piezoelectric perovskites. Science and Technology of Advanced Materials. 2015;**16**:046001-0460016

[66] Mir LL, Frontera C, Aramberri H, Bouzehouane K, Fernandez JC, Bozzo B, et al. Anisotropic sensor and memory device with a ferromagnetic tunnel

barrier as the only magnetic element. Scientific Reports. 2018;**8**:861-870

[67] Xu Y, Memmert U, Hartmann U. Magnetic field sensors from polycrystalline manganites. Sensors and Actuators A. 2001;**91**:26-29

[68] Zhao T, Ogale SB, Shinde SR, Ramesh R, Droopad R, Yu J, et al. Colossal magnetoresistive manganite-based ferroelectric field-effect transistor on Si. Applied Physics Letters. 2004;**84**:750-752

[69] Nuraje N, Su K. Perovskite ferroelectric nanomaterials. Nanoscale. 2013;**5**:8752-8780

[70] Mitra C, Raychaudhuri P, Kobernik G, Dorr K, Muller KH, Schultz L, et al. p-n diode with hole- and electron-doped lanthanum manganites. Applied Physics Letters. 2001;**79**:2408-2410

[71] Munoz JLG, Frontera C, Murias BR, Mira J. Dielectric properties of $Bi_{1-x}Sr_xMnO_3$ (x = 0.40, 0.50) manganites: Influence of room temperature charge order. Journal of Applied Physics. 2009;**105**:084116-084120

[72] Sleight AW, Gillson JL, Bierstedt PE. High-temperature superconductivity in the $BaPb_{1-x}Bi_xO_3$ system. Solid State Communications. 1993;**88**:841-842

[73] Manh DH, Phong PT, Nam PH, Tung DK, Phuc NX, Lee IJ. Structural and magnetic study of $La_{0.7}Sr_{0.3}MnO_3$ nanoparticles and AC magnetic heating characteristics for hyperthermia applications. Physica B. 2014;**444**:94-102

[74] Ding R, Li X, Shi W, Xu Q, Han X, Zhou Y, et al. Perovskite $KNi_{0.8}Co_{0.2}F_3$ nanocrystals for supercapacitors. Materials Chemistry A. 2017;**5**:17822-17827

[75] Mahata MK, Koppe T, Mondal T, Brusewitz C, Kumar K, Rai VK, et al. Incorporation of Zn^{2+} ions into $BaTiO_3:Er^{3+}/Yb^{3+}$ nanophosphor: An effective way to enhance upconversion, defect luminescence and temperature sensing. Physical Chemistry Chemical Physics. 2015;**17**:20741-20753

[76] Ho WJ, Li GY, Liu JJ, Lin ZX, You BJ, Ho CH. Photovoltaic performance of textured silicon solar cells with $MAPbBr_3$ perovskite nanophosphors to induce luminescent down-shifting. Applied Surface Science. 2018;**436**:927-933

[77] Singh DK, Manam J. Structural and photoluminescence studies of red emitting $CaTiO_3:Eu^{3+}$ perovskite nanophosphors for lighting applications. Journal of Materials Science: Materials in Electronics. 2016;**27**:10371-10381

[78] Kumar KN, Vijayalakshmi L, Choi J. Investigation of upconversion photoluminescence of $Yb^{3+}/Er^{3+}:NaLaMgWO_6$ noncytotoxic double-perovskite nanophosphors. Inorganic Chemistry. 2019;**58**:2001-2011

[79] Tian Y, Zhou C, Worku M, Wang X, Ling Y, Gao H, et al. Highly efficient spectrally stable red perovskite light-emitting diodes. Advanced Materials. 2018;**30**:1707093-1707097

[80] Jain N, Singh RK, Sinha S, Singh RA, Singh J. Color tunable emission through energy transfer from Yb^{3+} co-doped $SrSnO_3:Ho^{3+}$ perovskite nano-phosphor. Applied Nanoscience. 2018;**8**:1267-1278

[81] Li X, Zhang Q, Ahmad Z, Huang J, Ren Z, Weng W, et al. Near-infrared luminescent $CaTiO_3:Nd^{3+}$ nanofibers with tunable and trackable drug release kinetics. Journal of Materials Chemistry B. 2015;**3**:7449-7456

[82] Itoh S, Toki H, Tamura K, Kataoka F. A new red-emitting phosphor, $SrTiO_3:Pr^{3+}$ for low-voltage electron excitation. Japanese Journal of Applied Physics. 1999;**38**:6387-6391